

Modeling arrival scattering due to surface roughness

Orlando C. Rodríguez¹, António J. Silva¹, João Pedro Gomes², Sérgio M. Jesus¹

¹Instituto de Sistemas e Robótica, Campus de Gambelas, Universidade do Algarve, {orodrig,asilva,sjesus}@ualg.pt

²Instituto de Sistemas e Robótica, Instituto Superior Técnico, jpg@isr.ist.utl.pt

Signal scattering due to surface roughness constitutes one of the most important modeling problems in underwater acoustics when dealing with signal processing at large frequencies (i.e. above 1 kHz). Such modeling requires, in particular, realistic predictions of the ocean surface, which is usually perturbed by the propagation of swells and wind driven surface waves. Most of experimental studies had been dealing with short-range propagation, although it still remains unclear the separated impact of periodic vs. stochastic surface roughness on the arrival structure of received signals. The main purpose of the discussion presented in this paper is to clarify such issues through the calculation of impulse responses at high frequencies, at short and large ranges, using a ray tracing acoustic propagation model. The results of the simulations are expected to improve strategies of signal processing when scattering affects the received signal.

1 Introduction

Arrival scattering due to surface roughness represents one of the most important problems in the propagation of high frequency acoustic signals in underwater acoustics. It is in fact a complex theoretical and technical problem, of importance for the transmission and/or exchange of information between surface and/or underwater vessels. Besides signal scattering on the surface the underwater channel exhibits a complex behaviour due to multipath propagation and multipath generation and fading; the waveguide is affected by source and/or receiver motion, bottom bathymetry, and range dependency of the sound speed field. Sea surface can be perturbed by the propagation of periodic-like waves as swells, or stochastic perturbations like wind-driven surface waves. Surface roughness depends on many environmental factors (like wind conditions, near-surface presence of bubbles, etc.), and changes fast enough to affect the waveguide along transmissions[1]. Therefore, at high frequencies the sea surface is a source of motion, inducing stochastic Doppler effects on the signal frequency. The combination of Doppler with multipath propagation turns the propagation channel into a doubly spread channel, which can be characterized by the so-called *scattering function*. The scattering function can be used to determine, at the receiver, the expected correlation response to the propagation of the signal in a stochastic linear time-varying system. The knowledge of the scattering function allows also to optimize receiver and transmitter parameters[2], which is one of the main goals for source detection and underwater communications. However, despite the extensive material dedicated to the discussion of scattering functions due to surface motion there are a few questions, which seem to have been addressed in a somehow fuzzy manner, making unclear the relationship between Doppler spreads, ray structure and wind direction. The main purpose of this paper is to develop a brief theoretical review concerning signal scattering induced by variable sea surfaces, and to present a set of ray tracing simulations, that model the impact of surface scattering

on received signals. Such modeling is developed for both periodic-like and stochastic sea surfaces, at short ranges, considering a real shallow water range dependent waveguide. The simulations allow to improve the general understanding of Doppler spreads. The conclusions and future work are presented at the end of the paper.

2 Theory

2.1 Signal propagation in a doubly channel

Let us consider a propagation channel, which can be modeled as a stochastic linear time-varying system, with impulse response $h(t, \tau)$, which describes the response of the system at time t to an impulse applied τ seconds later. Therefore, if the input to the channel is a signal $s(t)$, then the output $x(t)$ can be written as a time varying convolution[3]:

$$x(t) = \int_{-\infty}^{\infty} h(t, \tau) s(t - \tau) d\tau. \quad (1)$$

Taking the Fourier transform of $h(t, \tau)$ with respect to t allows to calculate the spreading function:

$$S(\phi, \tau) = \int_{-\infty}^{\infty} h(t, \tau) e^{-j2\pi\phi t} dt, \quad (2)$$

which determines the amount of spread in delay τ and Doppler ϕ that an input signal undergoes in passing through a time-varying linear channel. Substitution of Eq.(2) into Eq.(1) allows to obtain that

$$x(t) = \int_{-\infty}^{\infty} \int_{-\infty}^{\infty} S(\phi, \tau) s(t - \tau) e^{j2\pi\phi t} d\tau d\phi, \quad (3)$$

which indicates that the output $x(t)$ corresponds to a weighted sum of delayed and Doppler shifted replicas of the transmitted signal.

2.2 The WSSUS conditions and the scattering function

Under wide sense stationary and uncorrelated scattering (WSSUS) conditions one can consider that the spreading function is uncorrelated with itself in delay and Doppler[4], so the autocorrelation of the input signal corresponds to

$$R_{ss}(\tau, \tau_1, \phi, \phi_1) = E \left[|S(\tau, \phi)|^2 \right] \delta(\tau - \tau_1) \delta(\phi - \phi_1) \equiv R_s(\tau, \phi) \delta(\tau - \tau_1) \delta(\phi - \phi_1), \quad (4)$$

where $R_s(\tau, \phi) = E \left[|S(\tau, \phi)|^2 \right]$ is the *scattering function*. It is a real positive function of τ and ϕ and can be considered as an average power density function, which determines the average amount of spread in frequency ϕ and delay τ that a waveform energy will suffer as the signal propagates through the doubly channel.

2.3 Rayleigh roughness parameter

From an acoustic point of view surface roughness can be characterized through the Rayleigh roughness parameter [1]:

$$R = 2k\sigma \sin \theta = \frac{4\pi\sigma \sin \theta}{\lambda} \quad (5)$$

where σ represents the RMS surface-wave height (crest to trough), θ is the grazing angle, λ is the acoustic wavelength and k is the wavenumber ($k = 2\pi/\lambda$). When $R \ll 1$ the surface is primarily a *reflector* and produces a coherent reflection at the specular angle equal to the angle of incidence; when $R \gg 1$ the surface acts as a *scatterer*, sending incoherent energy in all directions. Reflectivity from a rough boundary can be characterized through the relationship [5]

$$\mathfrak{R}'(\theta) = \mathfrak{R}(\theta) \exp\left(-\frac{R^2}{2}\right). \quad (6)$$

where \mathfrak{R}' and \mathfrak{R} stand for the new and old reflection coefficients, respectively, with \mathfrak{R}' being reduced because of scattering at the rough interface.

2.4 Spectra of wind-driven sea surface waves

A characterization of a wind-driven sea surface is given by the Pierson-Moskowitz spectrum [6, 7]:

$$S(f) = \alpha \frac{g^2}{(2\pi)^4 f^5} \exp\left[-\frac{5}{4} \left(\frac{f_m}{f}\right)^4\right], \quad (7)$$

where

$$f_m = 0.13 \frac{g}{v} \quad (8)$$

is the peak's frequency, v represents the wind velocity, $g = 9,8 \text{ m/s}^2$ and $\alpha = 8,1 \times 10^{-3}$ is Phillip's constant; the quantity

$$T_p = \frac{1}{f_m} = \frac{v}{0.13g} \quad (9)$$

represents the peak's period. The Pierson-Moskowitz spectrum is intended to represent a fully developed wind generated sea and it is valid in the interval $10 \text{ m/s} < v < 20 \text{ m/s}$. Another alternative is given by the JONSWAP spectral model [8]:

$$S(\omega) = \alpha' g^2 \omega^{-5} \exp\left[-\frac{5}{4} \left(\frac{\omega}{\omega_p}\right)^4\right] \gamma^\delta, \quad (10)$$

where δ is a peak enhancement factor:

$$\delta = \exp\left[-\frac{(\omega - \omega_p)^2}{2\sigma_0^2 \omega_p^2}\right]. \quad (11)$$

The parameters γ and σ_0 are given as $\gamma = 3.3$, $\sigma_0 = 0.07$ for $\omega \leq \omega_p$ and $\sigma_0 = 0.09$ for $\omega > \omega_p$, while α' is function of fetch X and wind speed v :

$$\alpha' = 0.076 \left(\frac{gX}{v}\right)^{-0.22}, \quad (12)$$

and peak frequency ω_p is given by

$$\omega_p = 7\pi \left(\frac{g}{v}\right) \left(\frac{gX}{v^2}\right)^{-0.33}. \quad (13)$$

Wave height and speed

Surface wave height can be related to wind speed through the well-known Beaufort scale. For deep water propagation the phase speed of the surface wave is calculated as

$$c_p = \frac{g}{\omega_p} \quad (14)$$

while the group speed corresponds to

$$c_g = \frac{1}{2} c_p. \quad (15)$$

Frequency to wavenumber conversion

The spectra described are defined in the frequency domain. For acoustic propagation is preferable to generate realizations of the sea surface in space rather than in time, which requires the spectra to be defined in the wavenumber domain. The conversion from frequency to wavenumber can be accomplished by taking into account that

$$E(k)dk = S(f)df, \quad (16)$$

where $S(f)$ represents the spectrum in the frequency domain and $E(k)$ represents the spectrum in the wavenumber domain. For surface waves over deep oceans frequency and wavenumber can be related as

$$\omega = \sqrt{gk}, \quad (17)$$

which allows to obtain the relationship

$$\frac{df}{dk} = \frac{1}{4\pi} \sqrt{\frac{g}{k}}. \quad (18)$$

Thus, the spectrum in the wavenumber domain can be calculated from the spectrum in the frequency domain as

$$E(k) = \frac{1}{4\pi} \sqrt{\frac{g}{k}} S(f). \quad (19)$$

Generally speaking the peak spectrum shifts towards lower wavenumbers (i.e. longer wavelengths) as wind speed increases. Therefore, high values of wind speed induce the propagation of low-frequency surface waves, associated with larger amplitudes and more energy transfer to the ocean.

Angular spreading

The directivity of wind speed can be incorporated into the modeling by introducing a spreading function along different angles; the full spectrum can then be written as

$$F(k, \theta) = E(k)D(f, \theta), \quad (20)$$

where $D(f, \theta)$ represents the spreading function. Since the total energy in the directional spectrum should be the same as the total energy in the one-dimensional spectrum a fundamental condition for the choice of the function $D(f, \theta)$ is that

$$\int_{-\infty}^{\infty} \int_{-\pi}^{\pi} E(k)D(k, \theta) d\theta dk = \int_{-\infty}^{\infty} E(k) dk \quad (21)$$

Some of the most common spreading functions are presented in the following sections.

Cosine-squared spreading function

The cosine-squared sea surface spreading (which is independent of frequency) is given by the expression [9, 10]

$$D(\theta) = \begin{cases} \frac{2}{\pi} \cos^2(\theta - \theta_0) & -\frac{\pi}{2} + \theta_0 < \theta < \frac{\pi}{2} + \theta_0, \\ 0 & \text{otherwise,} \end{cases} \quad (22)$$

where θ_0 represents the wind's direction. The cosine-squared spreading function is strongly non-isotropic and different from zero only in the region where $|\theta - \theta_0| < \pi/2$.

Mitsuyasu spreading function

The Mitsuyasu sea surface spreading can be written compactly as [11]

$$D(f, \theta) = \frac{\Gamma(s+1)}{2\sqrt{\pi}\Gamma(s+1/2)} \left[\cos^2\left(\frac{\theta - \theta_0}{2}\right) \right]^s, \quad (23)$$

where $\Gamma(s)$ represents the Gamma function; the parameter s controls the angular distribution of energy along frequency as follows:

$$s = \begin{cases} 9,77 (f/f_m)^{-2,5} & f \geq f_m, \\ 6,97 (f/f_m)^5 & f < f_m; \end{cases} \quad (24)$$

the definition of s reflects the increase of the parameter near the peak spectral frequency and its decrease at low frequencies.

Hasselmann spreading function

The Hasselmann sea surface spreading can be written compactly as [6, 12]

$$D(f, \theta) = \frac{1}{N_p} \left[\cos^2\left(\frac{\theta - \theta_0}{2}\right) \right]^p; \quad (25)$$

through a maximum likelihood technique collected data was fitted to analytical expressions in order to obtain the following dependence of the parameters on frequency:

$$p = 9,77 \left(\frac{f}{f_m} \right)^\mu \quad (26)$$

and

$$\mu = \begin{cases} 4,06 & f < f_m, \\ -2,34 & f > f_m; \end{cases} \quad (27)$$

the normalization factor corresponds to

$$N_p = 2^{1-2p} \pi \frac{\Gamma(2p+1)}{\Gamma^2(p+1)} \quad (28)$$

where $\Gamma(p)$ stands again for the Gamma function.

2.5 Swells

A swell is a long-wavelength surface wave, which is far more stable in his direction and frequency than normal wind-induced surface waves. Swells are often created by storms thousands of nautical miles away from the areas where they are observed. Such large distances allows the waves comprising the swells to become more stable and clean as they travel toward the coast. The level of energy contained in swells is influenced by the following factors: wind velocity, wind area (i.e. the amount of ocean surface area which is affected by wind blowing in the same direction, also known as fetch), and wind duration. During a typical open ocean winter storm wind speed can achieve up to 23.15 m/s, blowing over 1000 km for 36 hours will produce a periodic swell with a characteristic period of 17-20 s. Swell characteristics can be predicted using ocean surface models as the NOAA (National Oceanic and Atmospheric Administration) ocean surface model WAVEWATCH III.

3 Simulations

3.1 The environment

The environment used for simulations corresponds to the shallow water range-dependent propagation scenario used in the UAN simulator[13] (see Fig.1). It corresponds to a rectangle of 20 by 25 km, with a depth variation of 180 m from the lower left corner to 20 m at the upper right corner. The Elba island is located at the origin. The averaged sound speed profile is shown in Fig.2; it exhibits a strong thermocline near 20 m, which prevents most of the acoustic energy to reach the surface before being refracted back to the bottom.

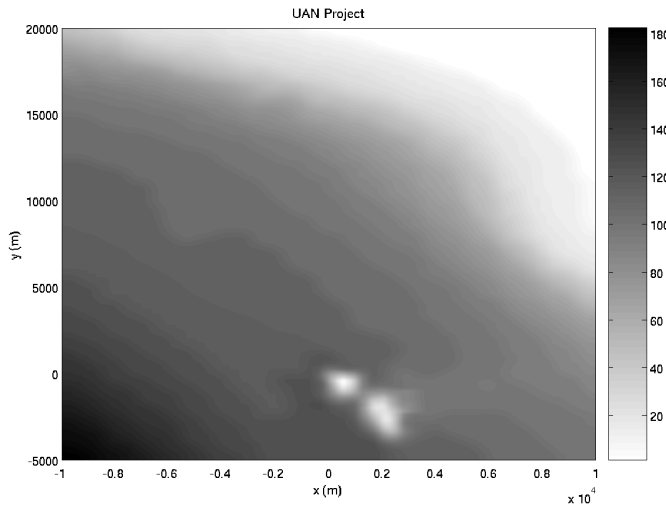


Figure 1: Waveguide bathymetry used in the simulations.

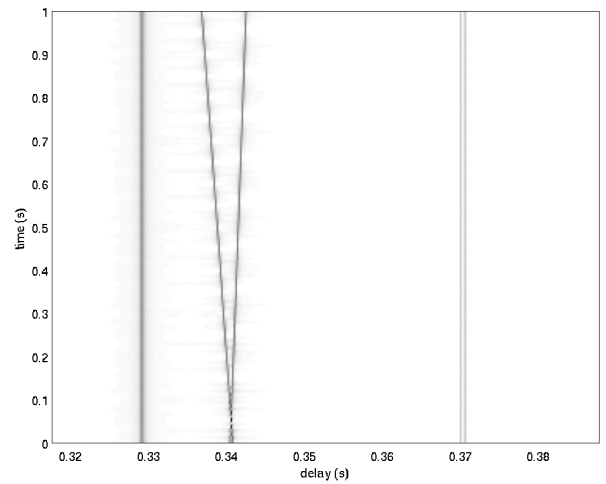


Figure 2: Waveguide sound speed profile.

3.2 Simulation setup

The simulations were directed to the identification of relationships between Doppler spreads, ray paths, surface characteristics and wave direction. In all cases the well-known Bellhop ray tracing model[14] was used.

Relationship between Doppler spread and delay perturbations

Doppler spread can be related to variations in delay time through a synthetic (although unrealistic) linear variation of arrivals; for a static (i.e. flat surface) configuration one can pick a pair of resolved arrivals, and shift the delays progressively in opposite directions along idealized transmissions. Such progressive shift of delay time can be followed by the calculation of the scattering function. In order to

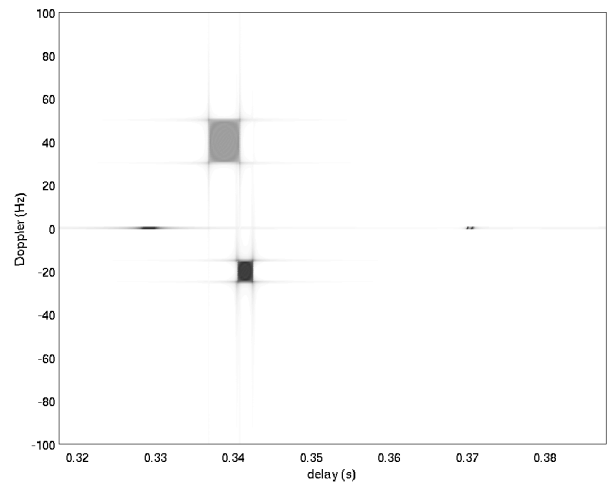


Figure 3: Synthetic variability of arrivals: transmissions along time (top); scatter function (bottom).

preserve direct arrivals the static configuration was chosen with the source located at coordinates (0,1000,60) m, and a single near-surface hydrophone at (0,1500,10) m. The synthetic perturbation can be seen in Fig.3(top). The calculation of the scattering function shows five well defined maxima (see Fig.3(bottom)). Without surprise the first and last two arrivals appear with zero Doppler spread. As for the arrival with decreasing delay the Doppler is positive (as if the source and the hydrophone were approaching each other), while for the increasing delay the Doppler is negative (as if the source and the hydrophone were moving away from each other). The temporal variation of arrivals is certainly unrealistic but it allows establish a clear interpretation of Doppler spreads in terms of delay variability: positive spreads represent a decrease of delay time along transmission time, while negative spreads can be seen as increases in arrival delay (and certainly symmetric spreads would correspond to a periodic variation of arrival delay). The next step consists in relating Doppler spreads to ray characteristics.

Swell surface wave propagation

Swells are ideal to relate Doppler spreads to ray characteristics since they can be idealized as single-tone periodic perturbations of the sea surface, whose phase changes progressively over time; therefore surface shape s can be modeled simply as

$$s(r, t) = A \sin(kr + \phi) \tag{29}$$

where A , k and $\phi(t)$ stand for the swell amplitude, wavelength and phase, respectively. A ray tracing using the parameters $A = 2$ m, $k = 2\pi/500$ rad/m and $\phi(t) = 0$ rad shows a configuration of eigenrays grouped in three pairs: pair one contains the direct and a single surface-bounced rays, pair three contains rays being reflected first on the bottom, pair two contains rays being reflected first on the surface (see Fig.4(top)).

As for the remaining paths they will exhibit positive or negative spreads according to the way their path is shortened or enlarged by a reflection on a wave crest or a wave trough. For paths with successive reflections on wave crests and troughs the spread will depend on how much a shortening by reflection on a wave trough will be compensated with an enlargement by reflection on a wave crest (a possibility even exists that such reflections can lead to the ray path being preserved). An additional ray tracing for an idealized swell of short wavelength, which induces an increase in local surface slope, reveals an structure of eigenrays similar to the previous one, but with many more rays arriving at the hydrophone (see Fig.4(bottom)). Such new rays can be interpreted as micropaths. However, one can expect that they will be very unstable, fading in and out in real data, as $\phi(t)$ changes progressively over time.

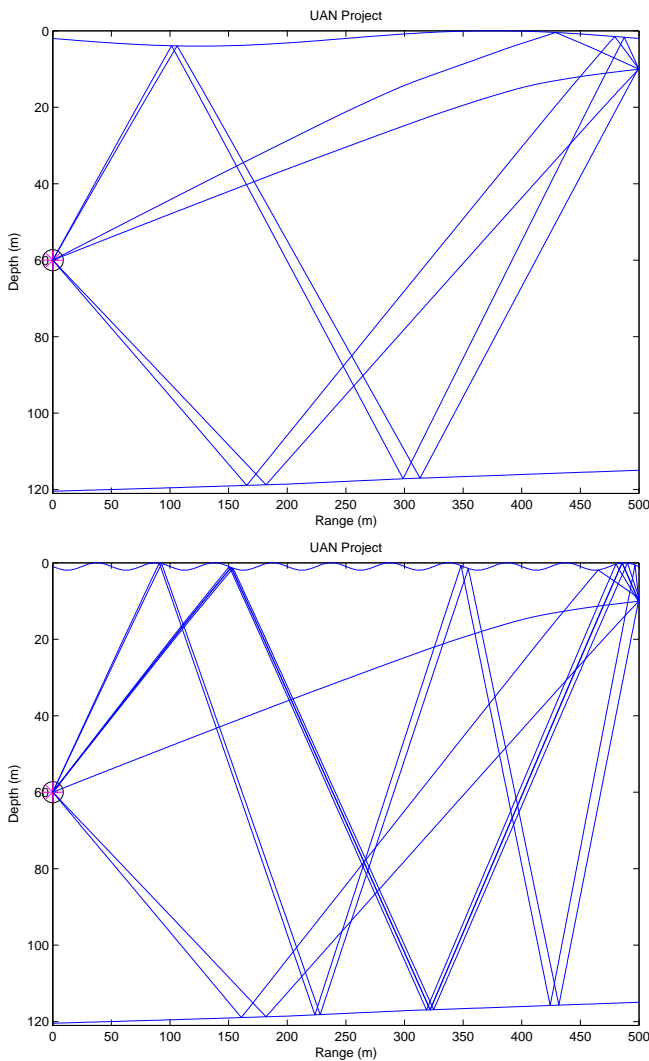


Figure 4: Idealized swell: impact on ray paths (top); formation of micropaths (bottom).

The direct and bottom bounced paths won't be affected by the propagation of the surface wave, and will be easily recognized in the scattering function as maxima with no spread.

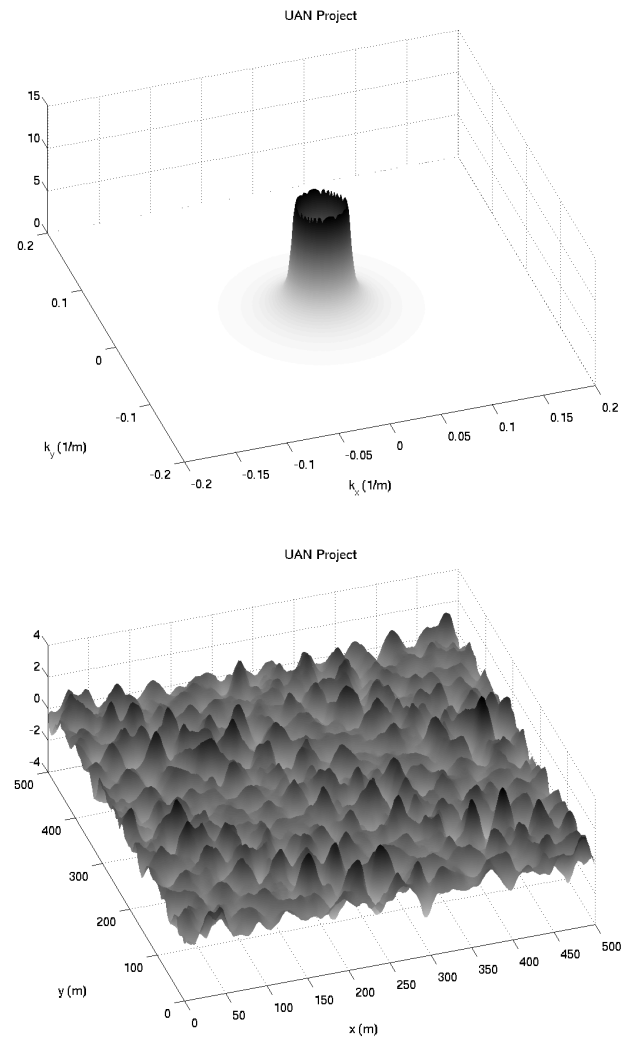


Figure 5: Sea surface waves for $v = 10$ m/s (no angular spreading): power spectrum (top); realization (bottom).

Wind-driven surface wave propagation

The procedure to generate sea surface realizations and to model their motion is described in [13]. A comparison of sea surfaces for $v = 10$ m/s ($T_p = 12.93$ s), $\theta_0 = 45^\circ$ with and without angular spreading is presented in Fig.5 and Fig.6. The uniform distribution of surface crests and troughs shown in Fig.5 is in sharp contrast with the directionality of the wavefronts of Fig.6.

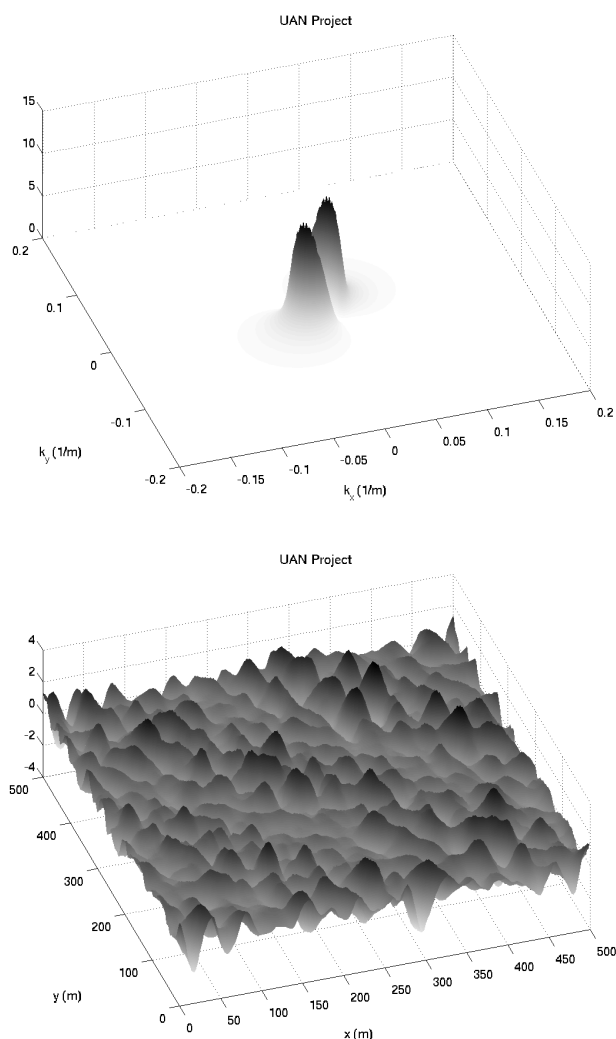


Figure 6: Sea surface waves for $v = 10$ m/s and $\theta_0 = 45^\circ$ (cosine-squared spreading): power spectrum (top); realization (bottom).

Delay perturbations along 4 seconds of transmission time, for the propagation geometry described in the previous section, and considering a sea surface like the one shown in Fig.5 can be seen in Fig.7(top). The direct and bottom-bounced arrivals can be seen as straight strips. The surface-bounced arrival appears oscillating back and forward, also with some fading along transmissions. Other paths appear

¹The angle of wind direction considered in all cases is taken relative to the X axis of the site bathymetry.

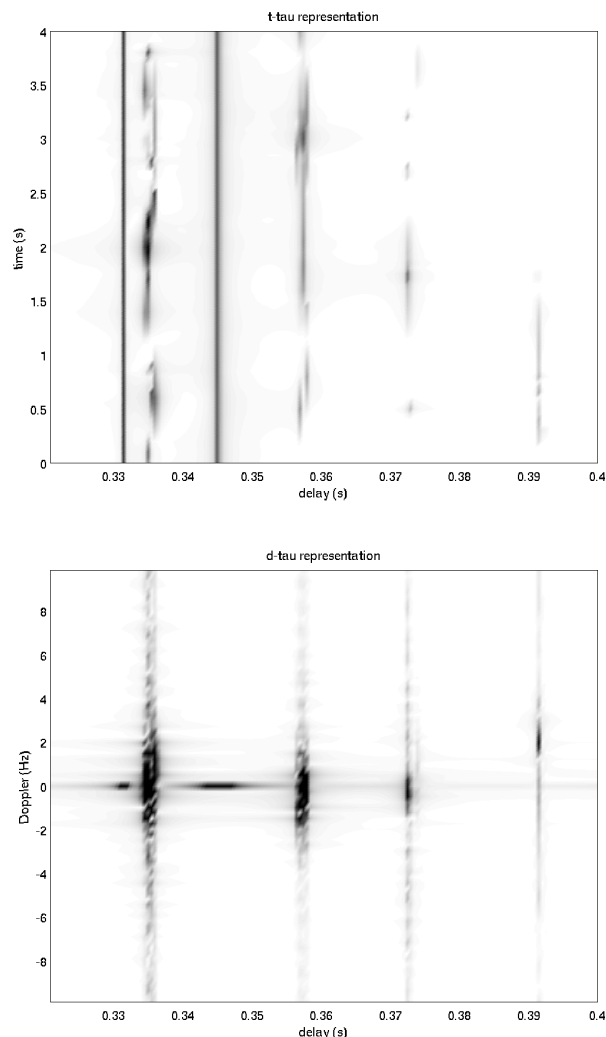


Figure 7: Simulation results for $v = 10$ m/s (no spreading): arrivals (top); scattering function (bottom).

with more unstable structures, but clearly different perturbations in delay. The scattering function shows two spots with zero spread corresponding to the direct and the bottom-bounced paths (see Fig.7(bottom)). Some smearing is present due to the fading in and out of arrivals. The single surface bounced path (near 0.335 s) appears with both positive and negative spreads, a consequence of progressive reflections on a wave trough or a wave crest; a similar behaviour is found in the spread of the single bottom bounced/single surface bounced path, near 0.36 s. As for last two arrivals (near 0.37 s and 0.39 s) one spread is negative, while the other is positive. Such behaviour is a consequence of multiple reflections on the sea surface, which induce the lengthening of the arrival at 0.37 s and the shortening of the arrival at 0.39 s.

The previous simulation did not account for the direction of propagation. The importance of this factor can be seen in Fig.8, which was obtained from simulations considering a sea surface propagating with $\theta_0 = 0^\circ$ (which is actually per-

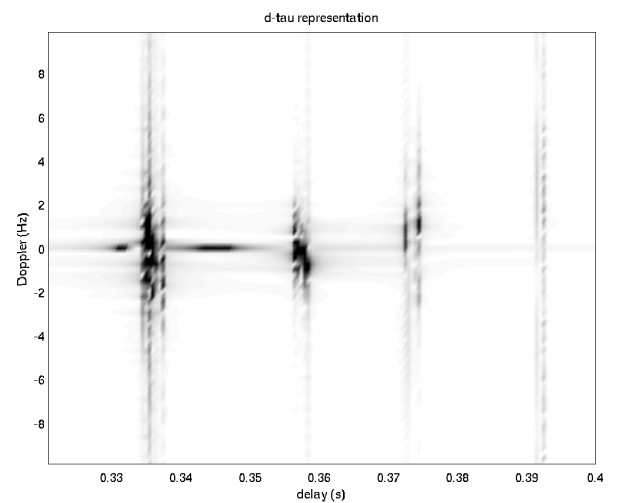
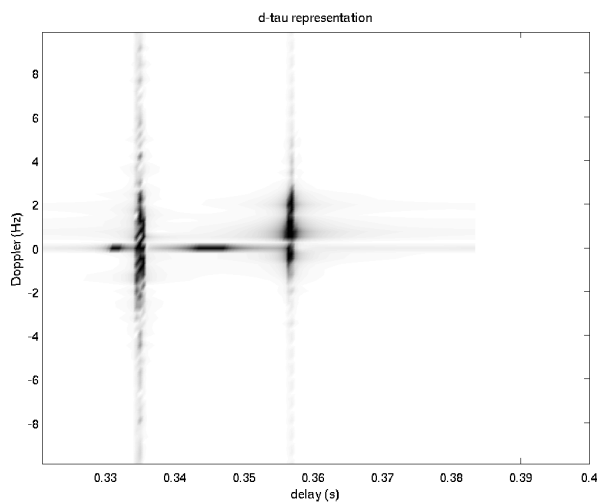
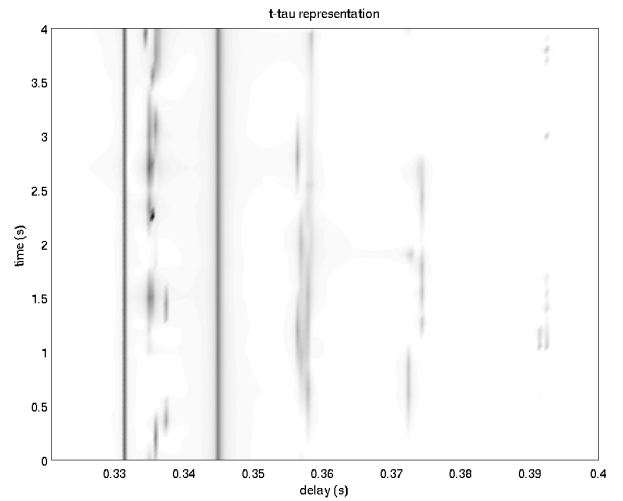
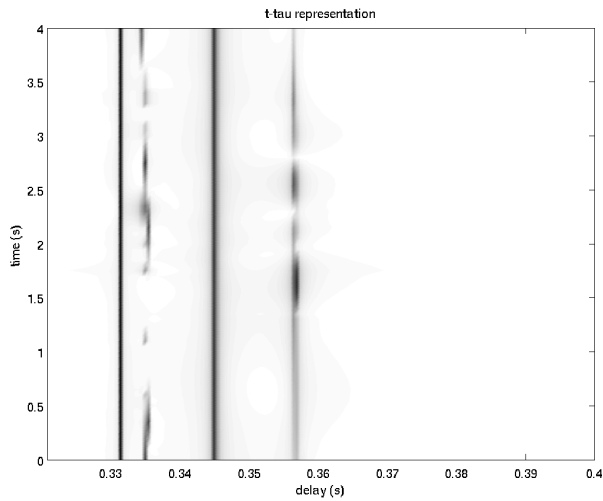


Figure 8: Simulations results for $v = 10$ m/s and $\theta_0 = 0^\circ$ (cosine-squared spreading): arrivals (top); scattering function (bottom).

Figure 9: Simulations results for $v = 10$ m/s and $\theta_0 = 45^\circ$ (cosine-squared spreading): arrivals (top); scattering function (bottom).

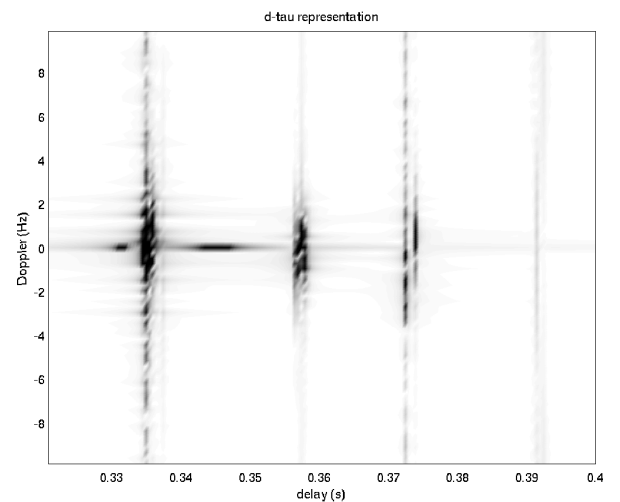
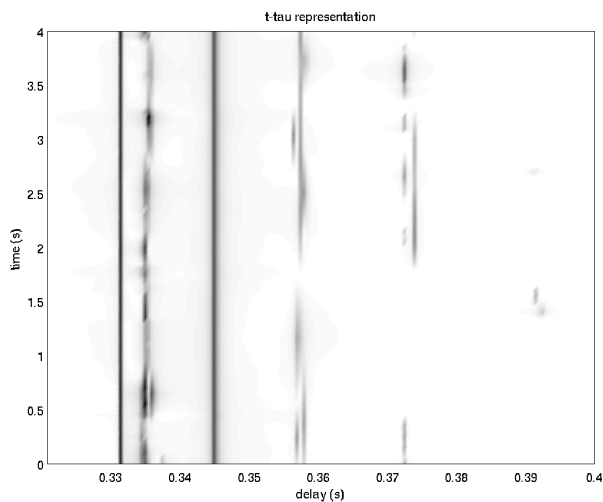


Figure 10(a): arrivals (same as Fig.9, but with $\theta_0 = 90^\circ$).

Figure 10(b): scattering function.

pendicular to the direction of acoustic transmissions). For such case the structure of arrivals appears to be very stable and the Doppler spread is practically absent (the smearing of spreads is just an artifact resulting from the sudden fading of some paths). Repeating the calculations for a sea surface propagating with $\theta_0 = 45^\circ$ allowed to obtain Fig.9, which exhibits a new pattern of arrival scattering: acoustic propagation along vertical transects of the surface wave that induce the generation of micropaths, which are stable enough to appear as positive spreads on the scattering function. Transmissions along the direction of the propagating surface wave seem to exhibit more stability in some of the previously unstable arrivals (see Fig.10). This not only enhances the spread exhibited by the scattering function, but reveals pairs of arrivals with opposite spreads.

4 Conclusions and future work

The discussion presented in this paper allowed to obtain a better understanding of arrival scattering due to the propagation of wind-driven sea surface waves. The connections between Doppler spread, ray structure and perturbation of delays along propagation time were modeled and discussed in detail for short ranges (i.e. acoustic propagation involving a direct path). However, further modeling will require extension to larger ranges, validation through comparison with real data and inclusion of additional factors, such as range and temporal dependencies of sound speed, source and/or array motion, and adaptation of the modeling results into processing systems of signal optimization.

5 Acknowledgement

This work is supported by European Commission's Seventh Framework Programme through the grant for Underwater Acoustic Network (UAN) project (contract no. 225669). It was also supported by the Portuguese Foundation for Science Technology under PHITOM (PTDC/EEA-TEL/71263/-2006) project.

References

- [1] Lord G.E. and Plemons T.D. Characterization and simulation of underwater acoustics signals reflected from the sea surface. *J. Acoust. Soc. America*, 63(2):378–384, February 1978.
- [2] Drumheller D.M. and Ricker D.W. Receiver-transmitter optimization for detection in doubly spread channels. *J. Acoust. Soc. America*, 89(4):1714–1723, April 1991.
- [3] Kay S. M. and Doyle S. B. Rapid Estimation of the Range-Doppler Scattering Function. *IEEE Transactions on Acoustic Speech and Signal Processing*, 51(1):255–268, January 2003.
- [4] Johnson B.L., Ricker D.W., and Sacha J.R. The use of iterative deconvolution for scattering function identification. *J. Acoust. Soc. America*, 91(5):2790–2798, May 1992.
- [5] Jensen F., Kuperman W., Porter M., and Schmidt H. *Computational Ocean Acoustics*. AIP Series in Modern Acoustics and Signal Processing, New York, 1994.
- [6] Mastin G. A., Watterberg P.A., and Mared J.F. Fourier Synthesis of Ocean Scenes. *IEEE Computer Graphics and Applications*, pages 16–23, March 1987.
- [7] Linnet L.M., Clarke S.J., Calder B.R., and Rzhano Y. The generation of a time correlated 2d random process for ocean wave motion. In *IPA97 IEEE Conference*, pages 623–625, July 1997.
- [8] Heitsenrether R.M. and Badiy M. Modeling Acoustic Signal Fluctuations Induced by Sea Surface Roughness. In *Proceedings of the High Frequency Ocean Acoustics Conference, AIP Conference Proceedings*, volume 728, pages 214–221, March 2004.
- [9] Coastal Engineering Technical Note. Technical note, U.S. Army Engineer Waterways Experimental Station, Coastal Engineering Research Center, P.O. Box 631 Vicksburg, Missisipi 39180, June 1985.
- [10] Chen-Fen Huang. *Acoustic Wave Scattering from Rough Sea Surface and Seabed*. Master Thesis, National Sun Yat-Sen University, 1998.
- [11] Mitsuyasu H. and Tsuyoshi U. A comparison of observed and calculated directional wave spectra in the east China sea. *Journal of the Oceanographical Society of Japan*, 45:338–349, September 1989.
- [12] Hasselmann D.E., Dunkel M., and Ewing J. A. Directional Wave Spectra Observed during JONSWAP 1973. *Journal of Physical Oceanography*, 10:1264–1280, August 1980.
- [13] Rodríguez O.C., Silva A.J., Zabel F., and Jesus S.M.M. The UAN interface: a web service for collaborative modeling. In *Proceedings of ECUA2010*, Istanbul, Turkey, July 2010.
- [14] Porter M. *The BELLHOP Manual and Users Guide*. HLS Research, La Jolla, CA, USA, 2010.